Applied Surface Science 741 (2026) 167089

Contents lists available at ScienceDirect

Applied Surface Science

journal homepage: www.elsevier.com/locate/apsusc

Full Length Article

Nature and pH-dependent surface chemistry of TiN in aqueous environment from ab-initio and machine learning accelerated simulations

Clara Saetta [a], Alessandro Bonardi [a], Riccardo Todisco [a], Ilaria Barlocco [b], Alberto Villa [b], Alessandro Morittu [c], Giovanni Maria Piccini [c], Giovanni Di Liberto [a,*]

[a] Dipartimento di Scienza dei Materiali, Università degli Studi di Milano-Bicocca, Via Roberto Cozzi 55, 20125 Milano, Italy
[b] Dipartimento di Chimica, Università degli Studi di Milano, Via Golgi 19 20133 Milano, Italy
[c] Dipartimento di Scienze Chimiche e Geologiche, Università degli Studi di Modena e Reggio Emilia, Via G. Campi 103, 41125 Modena, Italy

ARTICLE INFO

Keywords:
Density functional theory
Titanium nitride
Molecular dynamics
Machine learning interatomic potentials

ABSTRACT

The nature of surfaces in aqueous environment has crucial implications in a broad series of important processes in catalysis and materials chemistry. Titanium Nitride (TiN) is a widely applied system. The atomistic nature of its interface with water and its pH-dependent surface chemistry are rather unexplored. In this work, we used density functional theory calculations in conjunction with ab initio and machine learning molecular dynamics to investigate the nature of TiN in aqueous environment. We focused on the stable (1 0 0) TiN surface. Then, we adopted the grand canonical formulation of species in solution to study the acid-base equilibrium constants on the surface and we calculated the pH at the point of zero charge (pH_{PZC}), close to 3. We compared the predicted pH_{PZC} with experimental measurements on commercial TiN. We also predicted the dissociation free energy of water at 298 K which is ~0.5 eV, comparable to other materials such as TiO_2. The results of this study provide an atomistic description of the nature of TiN/H_2O interface. They provide some information on relevant aspects for materials chemistry and catalysis applications of TiN.

1. Introduction

Most chemical processes of interest occur at the surface of a material in water environment [1–3]. At the same time, the acid-base behavior of a surface in contact with water plays a crucial role [4–6]. A precise description of protonation and deprotonation equilibria at the interface facilitates the determination of surface charge as a function of pH, thereby revealing processes such as ion adsorption, charge transfer and catalytic activity [7–9]. Given that most technological applications involving functional materials are conducted in aqueous environment, it is imperative to elucidate the way water molecules interact with solid surfaces at the atomic scale. This interaction governs key interfacial phenomena, influencing both the stability of the material and its reactivity. In this context, the point of zero charge (PZC) is a particularly informative quantity. The PZC is defined as the pH at which the surface carries no net charge [10,11]. The ability to predict the PZC necessitates a comprehensive view of interfacial speciation and the ability to quantify the thermodynamics of proton transfer [12–15].

Several different approaches have been proposed over the years [16,17]. A way to access dynamic effects combines density functional theory (DFT) calculation with ab initio molecular dynamics (AIMD) [18–21]. Also, recently Machine Learning interatomic potentials emerged as a powerful frontier to scale-up AIMD simulation in both size and time scales [22–25]. Machine-Learning Molecular Dynamics (MLMD) allows in principle to propagate trajectories in the nanosecond regime in place of the picosecond one and at the same time to models of larger dimensions [26,27]. Besides the understanding of the nature of material/water interfaces, one of the most powerful approaches to access the pH-dependent surface chemistry relies on the Grand Canonical formulation of species in solution by Pasquarello and co-workers [18,28,29].

Titanium nitride (TiN) is quickly emerging as a cheap and valuable catalytic material for energy and environmental applications [30–33]. The TiN-water interaction remains relatively unexplored compared to oxides, despite its emerging role in applications such as electrocatalysis and energy conversion. An understanding of the interfacial chemistry between titanium nitride (TiN) and water is of fundamental relevance across several fields, including catalysis, electrochemistry, and materials

* Corresponding author.
E-mail address: giovanni.diliberto@unimib.it (G. Di Liberto).

https://doi.org/10.1016/j.apsusc.2026.167089
Received 13 February 2026; Received in revised form 18 April 2026; Accepted 30 April 2026
Available online 1 May 2026

science.

In this study, we performed DFT calculations in conjunction with AIMD and MLMD to investigate the pH-dependent surface chemistry of TiN in water. The findings of this study show that water preferentially adsorbs molecularly on the surface of TiN, with a low but non-zero degree of dissociation being expected. The assessment of the nature of TiN/water interface has been done by both AIMD and MLMD. Then, the acid-base properties have been investigated by means of the Grand Canonical formulation of species in solution, by working with AIMD. It is known that real TiN samples can be protected by thin TiO_x layers, an aspect which adds increasing complexity to the surface chemistry of real samples. This point goes beyond the specific purpose of this theoretical and fundamental work, that therefore represents a first but important preliminary step to access the experimental complexity of real samples. Interestingly, the calculated acidic constants at the surface were used to determine the pH_{PZC}, that were compared with the experimentally measured value of Dynamic Light Scattering (DLS) on commercial TiN [34,35]. Both measured and calculated pH_{PZC} are rather acid, around 3. This can be explained by assuming that the chemistry of TiN in real samples is not dramatically affected by the presence of a thin oxide protective layer, allowing to grasp valuable information from simplified models. In summary, the present study provides a comprehensive atomistic description of TiN/H_2O interactions and their effect on surface chemistry under variable pH conditions. The findings contribute to a broader understanding of transition metal nitride interfaces and pave the way for the rational optimization of TiN in aqueous-phase applications.

2. Computational details

2.1. DFT and AIMD calculations

Density functional theory calculations were performed by the VASP package [36]. The Perdew–Burke–Ernzerhof (PBE) exchange–correlation functional was employed [37]. Core electrons were treated with projector augmented wave (PAW) pseudopotentials [38]. Valence electrons were expanded over a plane-wave basis set with a kinetic cutoff equal to 400 eV. Electronic self-consistent field cycles were considered converged with a threshold equal to 10^{-5} eV. Ionic loops were stopped when the forces were lower than 10^{-2} eV/Å. Dispersion interactions were included using Grimme's D3 parametrization [39]. It must be mentioned that GGA functionals, such as PBE, are not the best solution to treat water. However, they have proven sufficiently reliable in capturing the pH-dependent surface chemistry of materials at an acceptable computational cost [18,40,41]. Also, the powerful machine learning universal foundation model described below has been obtained with DFT-PBE level of theory, which is a further justification for the choice of the functional. Ab initio molecular dynamics (AIMD) simulations were conducted at 350 K, regulated via a Nosé–Hoover thermostat [42,43]. The trajectories were first equilibrated for at least 5 ps followed by 25 ps of production run [20,44,45]. Previous works showed that about 8–10 ps trajectories allow to provide some insights on the nature of material/water interfaces, and to describe the solvation of chemical species [18,28,29,46–49].

Titanium Nitride (TiN) crystallizes in a cubic rock salt structure. The bulk structure of TiN was first fully optimized from experimental data, using a dense k-point mesh, equal to 5x5x5. A slab model was then created and optimized. We examined the most relevant low-index surface of TiN: the (1 0 0) slab [50,51]. The (1 0 0) face is the dominant one in TiN structures, which is a common outcome for rock-salt solids [52–57]. A five-layer thick low index (1 0 0) surface was modeled from the bulk structure, taking insight from a previous work [52]. Although extended surface defects, such as steps or edges, may also be pertinent in real systems, the present investigation focuses on the most likely termination to extract general trends. We constructed a 2 × 2 supercell of the TiN (1 0 0) surface and interfaced it with liquid water. The lattice parameters *a* and *b* of the simulation box are equal to 8.383 Å. A water slab approximately 4 nm thick was created, containing a number of water molecules sufficient to reproduce density of ~1 g·cm^{-3} in the bulk region. Due to the large size of the simulation box and large computational effort, the sampling of the reciprocal space was restricted to the Γ-point for AIMD. We performed benchmark simulations to better justify this unavoidable choice, by sampling a set of ten points from AIMD trajectories and performed single-point calculations with a fine (2x2x1) grid, finding acceptable deviations according to the accuracy of the DFT calculations, within 4 meV/atom. For TiN/H_2O interface, we evolved two AIMD trajectories [18]. In the first, the water molecules were initially placed in a molecular adsorption configuration and interacting with surface Ti sites, corresponding to a full (100%) coverage of Ti surface sites. In the second case, dissociated water molecules were considered, with OH groups bound to Ti atoms and H atoms adsorbed on nearby nitrogen sites of the surface, corresponding to a full (100%) coverage of Ti and N surface sites, by OH and H species respectively.

2.2. Machine learning accelerated dynamics of TiN/H_2O interface

Machine learning–accelerated molecular dynamics (MLMD) simulations were performed to extend the accessible time and length scales of the TiN/H_2O interface dynamics. All MLMD simulations were carried out using the LAMMPS package [58], employing periodic boundary conditions in all directions. In order to minimize the methodological discrepancies with the ab initio molecular dynamics simulations, the same temperature and integration time step adopted in the AIMD trajectories were used. A MACE [59] architecture machine learning potential has been trained *ad hoc* and used to describe interatomic interactions. The model was obtained by refining the mpa0 foundational model [60] through a finetuning procedure [61], using a dataset composed of 134 reference frames. For further information about the training set construction, see Section 3.2. This strategy was chosen to avoid producing a larger dataset for the training itself. It was performed using the default MACE training settings, namely a cutoff radius of 6 Å and a network architecture consisting of two interaction layers [60]. The training procedure was carried out in two sequential stages. In the first stage, the model was optimized using weight loss strongly biased toward force accuracy, with weights of 10^3 for energies and 10^4 for forces. In the second stage, the loss weights were adjusted to 10^3 and 10^2 for energies and forces, respectively, to improve the energetic description of the system. The quality and transferability of the resulting ML potential were evaluated using an independent validation set consisting of 100 frames extracted from a molecular dynamics trajectory previously generated with the foundational interatomic potential.

2.3. pH-dependent surface chemistry with Grand Canonical formulation of species in solutions

Acidic constants were obtained by invoking the Grand Canonical formulation of species in solution developed by Pasquarello and co-workers [18,28]. Previous studies have demonstrated that propagation times on the order of few ps are sufficient to capture key features of pH-dependent surface chemistry and to reproduce experimental points of zero charge for a variety of oxide materials [18]. However, it is known that longer simulation times are needed to better sample the configurational space of material/water interfaces [45,62]. For this reason, we decided to propagate trajectories for 25 ps, in line with other seminal studies [45,62]. The associated uncertainty, evaluated via block averaging analysis, was found as high as 0.1 eV, consistent with the typical accuracy of this methodology. Fig. 1 displays a representative snapshot of the TiN (1 0 0)/water interface.

On the surface of TiN, one could investigate the acidity associated with the following reactions:

$$N_sH^+ + H_2O_{(l)} \rightleftarrows N_s + H_3O^+_{aq} \quad (1)$$

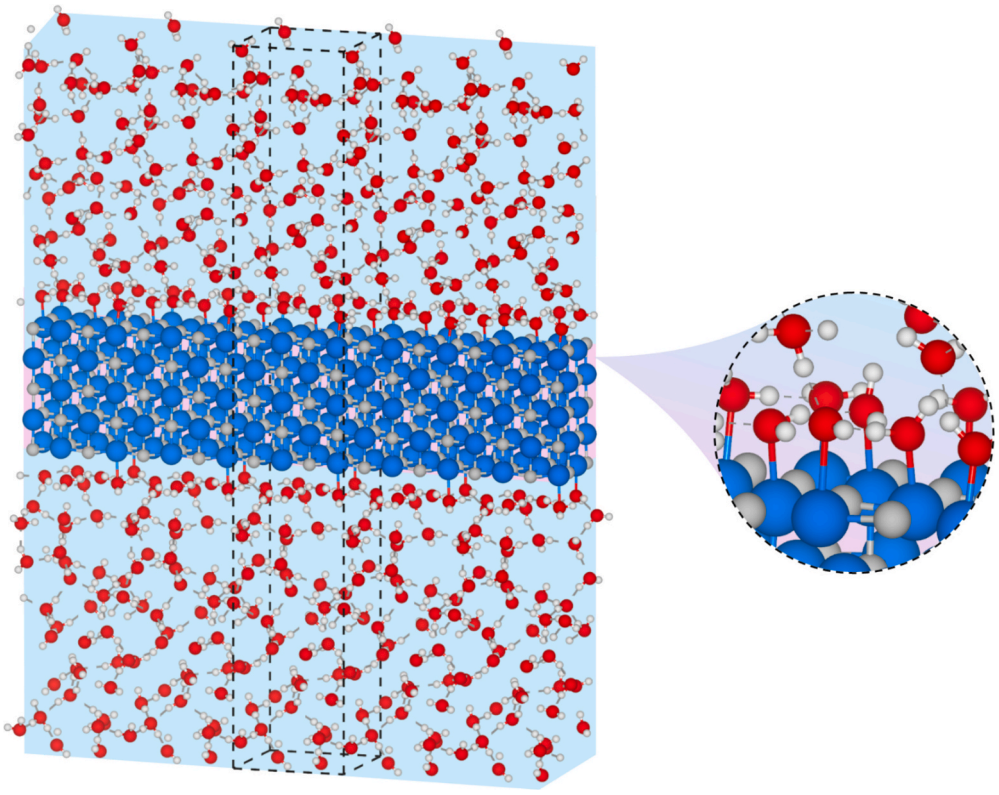

Fig. 1. Snapshot of TiN(1 0 0)/water interface. Dashed lines highlight edges of the simulation box.

$$H_2O_{Ti} + H_2O_{(l)} \rightleftarrows OH^-_{Ti} + H_3O^+_{aq} \tag{2}$$

where N_s stands for a generic surface nitrogen, N_sH^+ for a protonated surface nitrogen, H_2O_{Ti} for a water molecule adsorbed on a surface titanium atom and OH^-_{Ti} for an hydroxyl group adsorbed on a surface titanium.

These reactions are regulated by the following equilibrium constants, written in terms of concentrations approximating activities.

$$k_a(N_sH^+) = \frac{[N_s][H_3O^+]}{[N_sH^+]} = k_a^I \tag{3}$$

$$k_a(H_2O_{Ti}) = \frac{[OH^-_{Ti}][H_3O^+]}{[H_2O_{Ti}]} = k_a^{II} \tag{4}$$

On the surface of TiN, a proton from water can be attached to a surface nitrogen atom (N_sH^+), and a water molecule can absorb on a titanium one (H_2O_{Ti}). If we label the total number of exposed titanium and nitrogen sites as C_{Ti} and C_N, the pH corresponding to PZC (pH_{PZC}) is equal to [18]:

$$pH_{PZC} = \frac{pK_a(N_sH^+) - pK_a(H_2O_{Ti})}{2} - \frac{1}{2}\log\left(\frac{C_{Ti}}{C_N}\right) \tag{5}$$

The equations reported below describe the equilibrium constants [18]:

$$pK_a(N_sH^+) = \frac{[\Delta_{dp}A_{N_sH^+} - \Delta_{dp}A_{H^+}]}{k_bT\ln 10} + \frac{[-\Delta_{zp}A_{N_sH^+} + \Delta_{zp}A_{H^+}]}{k_bT\ln 10} + \frac{[V_w(int) - V_w]}{k_bT\ln 10} - \log c_0 \tag{6}$$

$$pK_a(H_2O_{Ti}) = \frac{[\Delta_{dp}A_{(H_2O)_{Ti}} - \Delta_{dp}A_{H^+}]}{k_bT\ln 10} + \frac{[-\Delta_{zp}A_{(H_2O)_{Ti}} + \Delta_{zp}A_{H^+}]}{k_bT\ln 10} + \frac{[V_w(int) - V_w]}{k_bT\ln 10} - \log c_0 \tag{7}$$

The first term represents the free energy change associated with deprotonation of a surface-adsorbed proton $\Delta_{dp}A_{N_sH^+}$, of a water molecule adsorbed on the surface $\Delta_{dp}A_{(H_2O)_{Ti}}$, with respect to the same property evaluated in acidic bulk water $\Delta_{dp}A_{H^+}$. The full derivation can be found in the original article by Pasquarello and co-workers [18] and in the ESI. Each term of the equations is averaged along AIMD simulation of TiN/water interfaces. In this regard, it must be mentioned that calculations remain meaningful, as results depend on energy differences arising from systems located in the same simulation cell and of equal charge [18]. The second term accounts for the zero-point energy correction. The third term reflects the difference in the macroscopic average of the electrostatic potential between the water side of the neutral TiN/water interface and that of bulk water [18]. The concentration of water molecules in the solution is taken as $c_0 = \frac{1000g}{18\frac{g}{mol}}$. Finite-size effects are neglected, as they are typically small (0.01–0.02 eV) in water and materials with high dielectric constants [18]. The same approach can be applied to evaluate the relative stability of molecular versus dissociative adsorption of water molecules. Specifically, the energy required to dissociate a molecularly adsorbed water molecule (ΔA_d) can be estimated as [18]:

$$\Delta A_d = k_bT\ln 10[pk_a^{II} - pk_a^I] \tag{8}$$

We assumed to work at $T = 298$ K. This approach is closely related to the widely adopted Computational Hydrogen Electrode (CHE) method, in which the free energy of water dissociation is estimated from minimum-energy structures, with thermodynamic corrections added afterward [63–68]. In contrast, the present methodology inherently accounts for the fluxional nature of interfacial water, capturing the presence of multiple low-energy local minima. Once the acid dissociation constants and the point of zero charge are determined, the concentrations of charged species and free surface sites can be evaluated as a function of pH. The molar fraction of surface species is then given by [18]:

$$\chi_{N_sH^+} = \frac{10^{-pH}}{k_a^I + 10^{-pH}} \quad (9)$$

$$\chi_{N_s} = \frac{k_a^I}{k_a^I + 10^{-pH}} \quad (10)$$

$$\chi_{H_2O_{Ti}} = \frac{10^{-pH}}{k_a^{II} + 10^{-pH}} \quad (11)$$

$$\chi_{OH^-_{Ti}} = \frac{k_a^{II}}{k_a^{II} + 10^{-pH}} \quad (12)$$

2.4. Experimental details

Commercial TiN (<3 μm) was purchased from Sigma-Aldrich and employed without any further treatments. Z-potential measurements were performed on Zetasizer lab from Malvern. 10 mg of support was dispersed in 50 ml of buffer solution and sonicated for 10 min. The buffers between pH 2 and 6 were prepared by employing the Britton-Robinson protocol [69]. Indeed, the same volume of H_3BO_3 0.04 M, CH_3COOH 0.04 M and H_3PO_4 0.04 M were mixed to obtain an acid solution (pH = 2). After that, NaOH 0.2 M was added dropwise to reach the desired pH. XRD patterns were recorded on a PANalytical X'PertPRO X-ray diffractometer. A Cu-Kα radiation source (40 kV and 30 mA) was utilized, and diffraction patterns were recorded between 20 and 80° 2θ with a step size of 0.02°/s. X-ray diffraction (XRD) measurements of commercial TiN confirmed that the material exhibits the characteristic features of the fcc cubic phase of TiN, in agreement with the expected crystal structure, Fig. S1 [70]. It must be underlined that despite (1 0 0) surface are typically stable in rock salt fcc cubic lattice of the type NaCl, such as TiN, they do not show intense (1 0 0) diffraction peak due to the well-known destructive interference effect. The average crystal size, as estimated from the XRD peak broadening was approximately 32 nm, validating the approximation of using a (1 0 0) surface model to describe the system at the atomic level.

3. Results and discussion

3.1. AIMD of TiN/H_2O interface

We start with the analysis of the neutral TiN(1 0 0)/H_2O interface. If we start with water molecularly adsorbed to the surface, after 25 ps of propagation, the fraction of dissociated water molecules on the surface reaches a value of about 6%, Fig. S2. If we propagate the trajectory starting from the opposite situation, i.e. water completely dissociated on the surface, after 25 ps of propagation, α decreases from 100% to 30%, Fig. S2. These two examples indicate the preferential molecular adsorption water on the surface, despite their different values are probably due to the need for very long simulation times to sample the fluxional nature of the solvent. The dissociation fraction was calculated by counting the number of species at the surface and by analyzing the Pair Distribution Functions (PDFs) and coordination numbers. Interestingly, we did not detect any dissociated species either fading away from the surface or in the bulk region of water. Fig. 2 shows the PDF between surface atoms and water for the trajectory starting with water molecularly adsorbed. The peaks located at 1.0 Å are associated with the direct interaction between surface nitrogen atoms (N_s) and hydrogen, due to water dissociation. The calculated coordination number is 0.06, in agreement with the fraction of water dissociated on the surface (see Table S1). Coordination numbers were calculated by integrating the PDF [71]. The value becomes 0.30 when starting the trajectory from dissociated water on the surface. We observe that surface N atoms are not prone to hydrogen bonding as can be evinced by the absence of any peak in the PDF_{NH} around 1.7 Å–2 Å. The PDF between titanium atoms and oxygen species shows a peak at 2.2 Å due to the interaction with

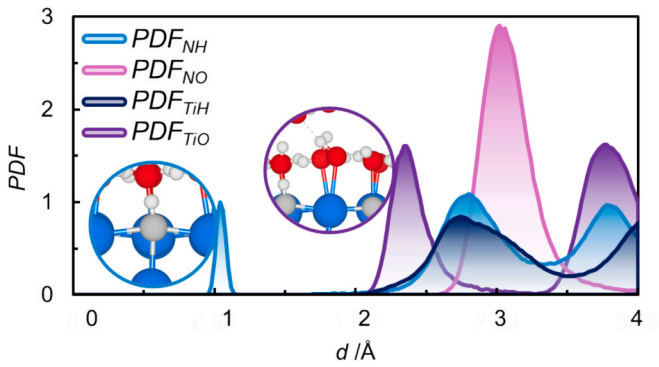

Fig. 2. Calculated pair distribution function (PDF) between N_s and H atoms (light blue), Ti_s and H atoms (dark blue), between N_s and O atoms (pink), Ti_s and O atoms (purple).

adsorbed H_2O or OH^- species arising from water dissociation (see Fig. S3). The calculated coordination number is 0.70, indicating that on average, about 70% of exposed Ti atoms are covered by water. To summarize this part, nitrogen atoms on the surface are not directly interacting with the solvent molecules via hydrogen bonding, at variance with transition metal oxide (TiO_2) [47,72]. On the other hand, exposed Ti atoms are highly covered by solvent molecules. We also calculated the free energy to dissociate water on the surface by using Eq.1 and 2 finding a value equal to 0.45 eV, which is comparable to the one of TiO_2 [47,72], indicating that molecular chemisorption is more favorable than dissociative one. These results are interesting in the optic of explaining this material behavior at the water interface.

3.2. Machine learning accelerated dynamics of TiN/H_2O interface

AIMD simulations are usually very computationally demanding. This limits the propagation time to few *ps*. This kind of propagation times (t < 30 ps) typically provides reliable results on the surface chemistry of materials [28,41,45,73]. At the same time, the high computational demand requires the adoption of a small cell sizes, leading to possible finite size effects. Finally, only a few trajectories can be propagated, an aspect that combined with the limited simulation time leads to possible dependence on the initial conditions. We trained Machine Learning potentials to tame the unavoidable limitations of AIMD simulations allowing for more realistic models and statistically sound simulations.

We prepared a fine-tuned potential, by defining a working dataset of points. The dataset used for fine-tuning was built up starting from the already performed AIMD simulations of TiN in aqueous environment, and other simulations. In particular, the data set was made by a total of 142 atomic configurations, subsequently divided into training (134 structures) and validation set (8 structures), selected to ensure both chemical and structural diversity. More precisely, 68 frames were extracted from the previously discussed AIMD trajectories of TiN in water (either molecularly or dissociative chemisorbed) by applying a diversity-based selection procedure using Smooth Overlap Of Atomic Positions (SOAP) descriptor [74], with the TiN atoms chosen as centers for the evaluation of dissimilarity. This strategy allowed us to avoid oversampling of the trajectories and ensuring that configurations with different dissociation fraction of water on the surface were included in the training set. The dataset was then augmented with additional configurations generated under conditions consistent with the AIMD simulations of the target system: 16 frames of bulk liquid water and 38 frames of bulk TiN were selected from independent AIMD trajectories carried out using the same temperature, level of theory, and integration parameters as the TiN-water simulations. This is fundamental in order to introduce relevant physical representations of the bulk region of the system under investigation [22]. Finally, to enrich the dataset with frames containing under-coordinated sites and thus getting a more

robust potential, 20 frames were extracted from a trajectory on a simple cubic TiN nanoparticle having a diameter of 1 nm interacting with water, performed with the MACE foundational model, by using the diversity-based selection procedure. The points were added to the dataset by performing DFT single-point calculations on top of each extracted frame. We observed that the inclusion of this type of points with high-energy under-coordinated sites, such as edges and vertices, allows to improve the stability and robustness of the potential. Once generated the fine-tuned potential, the accuracy was assessed by looking at both mean absolute error (MAE) on energy and forces with respect to reference data, that were sampled by a trajectory propagated with the foundation interatomic potential and extracting the 100 most-different configurations with SOAP. The starting configuration of the trajectory consisted of fully dissociated water at the TiN surface, to evaluate a set of points with a wide variety of dissociation fractions. When compared to the foundational mpa0 model, the fine-tuned potential showed a reduction of the energy error of about 70% and reduced standard deviation of the forces of about 50%.

Using this fine-tuned potential, we propagated trajectories for at least 1 ns after 100 ps of equilibration. This allowed us generalizing the results arising from AIMD simulations by taming the limitation of AIMD related to size effects, relatively short simulation times and dependence from initial conditions. As it will be detailed below, the MLMD simulations will also somewhat validate the previous findings. We first generated an expansion of the simulation box along a and b directions to assess the presence of possible spurious effects due to the limited size of AIMD simulation box. Fig. 3a and b report the calculated PDFs of atomic couples obtained from two different simulation boxes, $a = b = 8.383$ Å and $a = b = 16.766$ Å respectively. The starting configuration of the two trajectories is the same.

Interestingly, there are no sizeable changes in the position of the peaks related to Ti-O, N–H, O–H, and Ti-H contacts. Table S2 also reports the calculated coordination numbers, where we see that the use of a larger cell does not lead to changes with respect to the smaller one. Fig. 3c also reports the calculated dissociation fraction (α) of water molecules, where (without surprise) the trend of α for the larger size is smoother, due to the availability of a larger number of surface sites. Nevertheless, again, there is not sizeable change, as α is equal to 25%

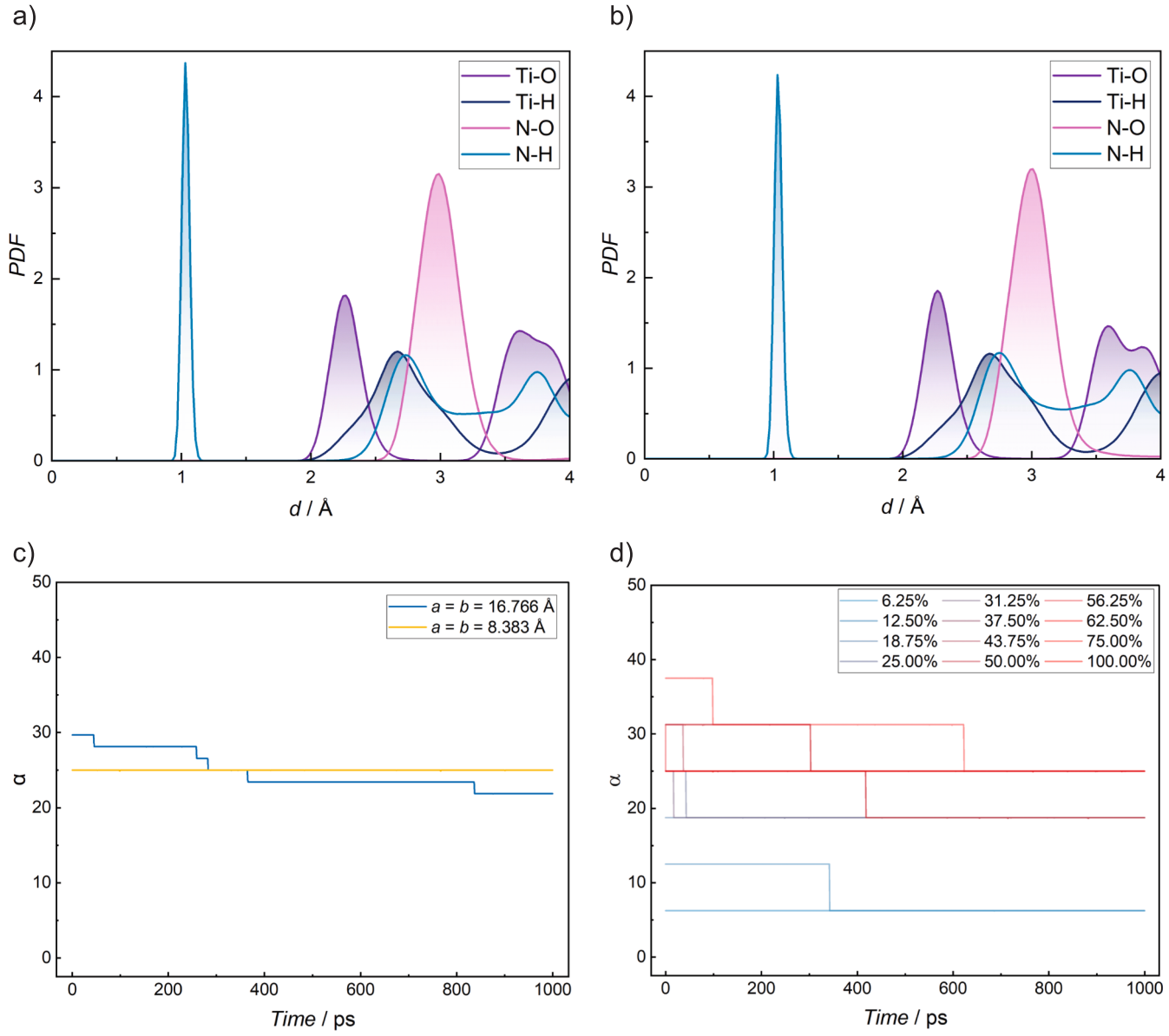

Fig. 3. Calculated PDFs for $a = b = 8.383$ Å simulation cell (panel a), $a = b = 16.766$ Å simulation cell (panel b), comparison between the water dissociation fraction (panel c) and trend in time of dissociation fraction for trajectories having different initial conditions (panel d).

and 22% for the smaller and larger cells. The data in Fig. 3d suggest that trajectories initialized with different dissociation fractions tend to converge toward similar but distinct steady-state values (~6% vs. ~20–25%). This behavior could be interpreted as evidence of the presence of two possible likely interfacial configurations, where very long simulation times could be needed or enhanced sampling techniques should be invoked to connect the two regions of the energy landscape. Indeed, disparate initial dissociation degrees may result in the formation of distinct hydrogen-bonding networks and local arrangements of OH/H species, which can stabilize a variety of interfacial states. Notably, regardless of the initial configuration, the overall dissociation fraction remains comparatively low, consistently suggesting a propensity for molecular water adsorption at the TiN interface. We also propagated other trajectories by changing the initial condition, in terms of fraction of water molecules dissociated on the surface, as detailed below. The analysis of the size effects of each trajectory is reported in Figs. S4–S15, and Table S2, where it can be appreciated that the results further corroborate the absence of relevant spurious size effects. Indeed, the maximum change in peak position of N–H, N–O, Ti–H, and Ti–O and coordination numbers is always very small, as high as 0.06 Å, and 0.14 for chemical interactions within 2.5 Å. This is an important result as it strengthens the reliability of the predictions and somewhat validates the working simulation box of AIMD, an aspect that will become relevant by evaluating the acidic constants at the TiN/H_2O interface.

AIMD simulations indicate that water preferentially coordinates to the surface molecularly, and dissociation occurs only partially. We assessed this aspect by looking at the longer simulations available by MLMD. We propagated a trajectory starting from completely dissociated water on the surface, and we analyzed the results after 1 ns and 25 ps of production run, following 100 ps of equilibration. Interestingly, α is equal to 25% when the trajectory is propagated for 1 ns, which is identical to the 25%, obtained by 25 ps only. This latter value is also consistent with 30% arising from AIMD. Fig. S16 also reports the calculated PDFs comparing MLMD with the two propagation times. From Table S2 one can appreciate that only negligible changes are present.

We repeated the same analysis, but started the trajectories from different initial configurations, having a variable fraction of dissociated water molecules. We propagated 12 trajectories. Fig. 3d shows the trend of the dissociation fraction in time of all the propagated trajectories. α most often approaches a value between 20 and 25% except for a couple of cases where it is smaller. The results are consistent by using larger simulation cells, Fig. S17. This analysis shows that the results are robust against the dependence from initial conditions.

A final aspect to address is the comparison between predictions obtained with short simulation times of 25 ps with respect to 1 ns one. We compared 1 ns propagation vs 25 ps in terms of PDF (Figs. S18-S29), trend of the dissociation fraction, and coordination numbers (Table S2) for all 12 propagated trajectories. In all cases, it can be appreciated that 25 ps allows to extract reliable information of the surface chemistry of TiN/H_2O interface. The MLMD results thus indicate that the adopted framework of AIMD allows us to retrieve reliable information on the nature of TiN/H_2O interface. This is a very important aspect providing motivation for the use of AIMD for the calculation of acidic constants and point of zero charge described below.

3.3. pH-Dependent surface chemistry

Once the nature of the TiN/H_2O water interface was assessed, we investigated the pH-dependent surface chemistry of TiN. This was done by propagating additional AIMD trajectories, one including an extra proton attached to the surface, and the second with a hydroxyl species generated by deprotonation of an adsorbed water molecule, to obtain the acidic constants and point of zero charge. It must be underlined that the simulation of charged cells does not introduce spurious effects as energy comparisons are performed between systems with the same total charge and cell [28,75,76]. For this specific purpose we could not work with Machine Learning potentials, as it would have been necessary to train a dedicated potential for the system in the presence of an extra proton and with hydroxyl. For this reason, we worked with AIMD trajectories, as the previous section showed that acceptable results can be extracted by AIMD propagated for 25 ps. In addition, dynamic light scattering (DLS) measurements were carried out to determine the pH_{PZC} of the TiN nanoparticles. Dynamic Light Scattering (DLS) is a widely used technique for measuring the zeta potential of colloidal particles in suspension and solid materials [77–79]. It works by applying an electric field to the sample and analyzing the Doppler shift in scattered light caused by the movement of charged particles. The resulting electrophoretic mobility is then used to calculate the zeta potential, which reflects the surface charge of the particles and their stability in suspension. DLS is particularly valuable for identifying the isoelectric point (IEP) providing key insights into the surface chemistry and colloidal behavior of nanomaterials. Formally, the point of zero charge (PZC) and isoelectric point (IEP) differ because the IEP depends on the electrostatic double layer at the shear plane, whereas the PZC depends only on the surface chemistry. In the absence of specific ion adsorption and for a simple, symmetric double layer, the two points can be considered approximately equal. We work under this approximation. A series of 5 buffer solutions with varying pH values (2–6) was employed to evaluate the isoelectric point of the particles.

Tables S3 and S4 report the working quantities and the calculated equilibrium constants and points of zero charge. The calculated pH_{PZC} of TiN (1 0 0) is 2.9, indicating slightly acid behavior. This value compares well with the value obtained with DLS analysis reported in Fig. 4a, within 2.5 and 3.0. This represents a remarkable agreement considering the unavoidable approximation adopted in the simulation models. Also, the obtained pH_{PZC} is also good agreement with other reported values. Chi-Jen Shih et al reported a value equal to 2 for TiN ultra-thin films and $pH_{PZC} = 4$ of pristine TiN [80]. Of course, experimental measurements reflect an average response across the different exposed facets and nanostructuring of TiN nanoparticles, which in turn is influenced by how the sample is prepared.

The calculated acidic constants can be used to evaluate the speciation on the surface as a function of pH, a relevant aspect for reactions such as water splitting. Fig. 4b shows how the molar fractions of surface sites change with pH, helping us identify the pH range in which different species are present at the surface. We applied a 10% threshold to determine when a species is considered relevant [18]. While the absolute values should be interpreted with some caution, the diagrams are still useful for spotting trends and making comparisons between different surfaces. By looking at Fig. 4b we see that H^+ ions are expected on the surface only in very acidic conditions, while at higher pH values, the surface nitrogen atoms are expected to be free. This is in line with the low dissociation fraction calculated for the neutral system. At the same time, OH^- ions display higher stability since they are present on the surface at pH > 6. Ti atoms tend to be covered by water in more acidic conditions.

3.4. Towards realistic TiN models

Overall, the results arising from AIMD and MLMD provide a description of how TiN interacts with water. Water preferentially coordinates molecularly to the surface atoms with only a partial dissociation. Titanium surface sites are nearly fully covered by O-atoms, either of H_2O or by OH species arising from water dissociation. This indicates that when putting TiN in a wet environment one can expect the formation of layers made by Ti-O motifs. These results also provide an atomistic description of the origin behind the formation of protective TiO_x layers that can be observed when putting TiN in an oxidizing environment [81–83]. In this regard, the outcomes of this study represent prerequisite information for future investigations focused on the nature of TiN/TiO_x/H_2O interfaces, where a thin TiO_x layer protects TiN.

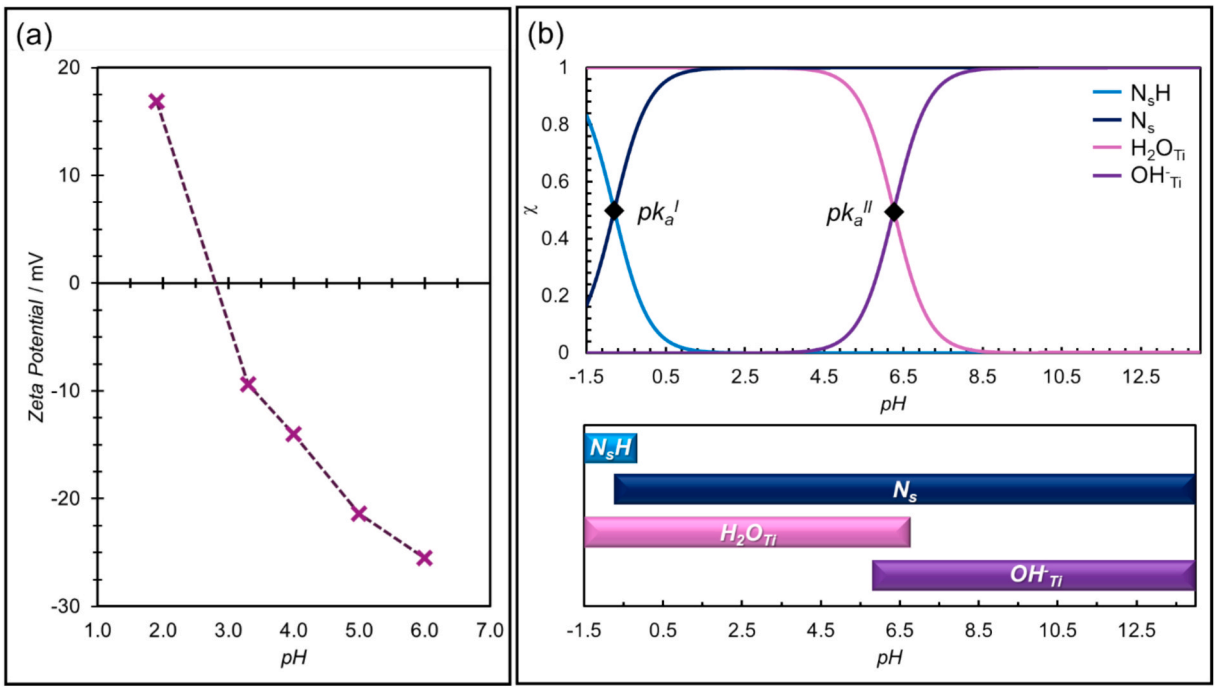

Fig. 4. (a) Z-potential experimental curve; (b) Speciation of adsorbed water (H_2O), free surface nitrogen sites (N_s), and H^+ and OH^- species as a function of pH on the surface of TiN (1 0 0); pH windows at which the H^+, N_s, H_2O, and OH^- species are present on the surface.

Given the importance of the aspect, in this study we perform preliminary simulation to gain atomistic insights on the nature of an oxide-protected TiN, in terms of structure of the interface and its interaction with water. The simulation of interfaces is extremely complex as it should involve very large models able to accommodate the structure of both units, with a negligible, ideally zero, lattice mismatch [84]. In the case of TiN/TiO_x, one needs to explore a series of degrees of freedom as the composition at the interface, the morphology and the thickness of the protecting unit [85,86]. Here, we explored two possible situations: i) the surface of TiN is covered by an extremely thin protective layer, where oxygen atoms saturate the coordination of exposed Ti ones, similar to what done by Qi Zhou et al [87]; ii) we considered the presence of TiO_x protective layer on the TiN surface. We first performed geometry optimizations without the presence of water, Fig. 5a and b.

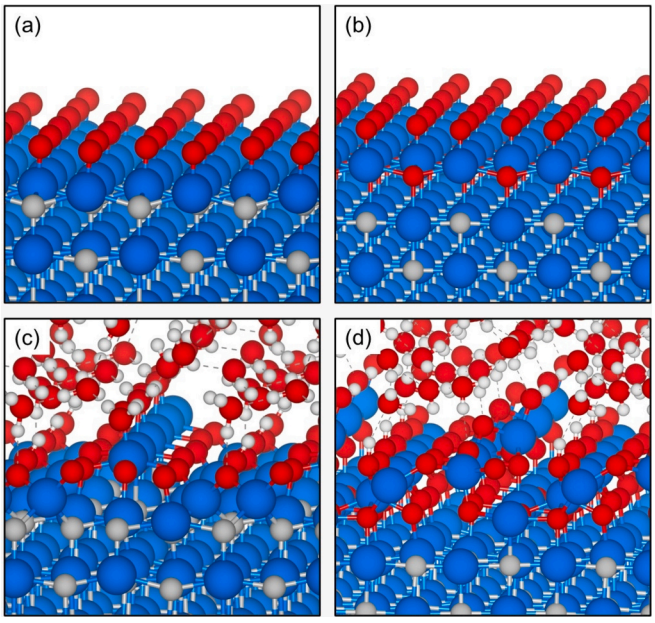

Fig. 5. (a) and (b) are for DFT optimized oxidized TiN models. Panel (c) and (d) are two snapshots from MLMD simulation of the same models after 100 ps.

The results of the optimizations were used as a starting point for MLMD simulations. In both cases the presence of TiO_x leads to a significant structural rearrangement during the dynamics, evolving towards an amorphous Ti-O overlayer, Fig. 5c and d. This result is interesting, as it shows the potential complexity of the TiN/TiO_x interface which will be governed by an amorphous region at the interface to better accommodate the structure of the composing units. Also, TiO_x serves as a protecting agent of TiN. This is confirmed by direct observation and the PDF for the N–H, Ti–O and O–H pairs (shown in Fig. S30), consistent with the known tendency of TiN to form native oxide films. In this case, the interaction of water with the fully TiO_x protected TiN is less intense. Oxygen atoms of water molecules are less frequently interacting with Ti, with a coordination number equal to 0.2 and 0.4 for the two oxidized models to be compared with 0.7 of the pristine surface interacting with water. At the same time, H atoms of water are not interacting with surface N atoms, but with oxygen species of the oxidized surface.

A possible explanation for the agreement between simulated pH_{PZC} of TiN/H_2O with experimental data could arise from the fact that the protective layer is not thick enough to strongly change the chemical nature of the TiN sample with respect to the ideal TiN material. Future work will be dedicated in the near future to deeply assess this question on the nature of TiN/TiOx interface and the impact to the surface chemistry, especially when very thick and robust layer of oxide covers the material.

4. Conclusion

In this study, we explored the pH-dependent surface chemistry of TiN in an aqueous environment using density functional theory in conjunction with ab initio and machine-learning accelerated molecular dynamics simulations. We first examined the nature of the interaction between water and material. We then used the grand canonical formulation of species in solution to estimate the acid-base equilibrium constants at the TiN/water interface. The resulting equilibrium constants

allowed us to estimate the point of zero charge (pH_{PZC}), a key experimental observable. We then validated the predicted pH_{PZC} with experimental measurements. Both theory and experiment show remarkable agreement with $pH_{PZC} \sim 3$. This information was used to study the pH-dependent speciation of H^+, OH^-, and H_2O on the surface of TiN, an important aspect to assess when looking at catalytic activity in reactions such as water splitting. It must be mentioned that all simulated results arise from calculations relying on a specific and perfect surface model of TiN. In this regard, some effects arising from the surface exposure and defects are possible. Future work will focus on extending this investigation to a broader spectrum of surface models, including also different types of defects and further better evaluating the water arrangement when nanostructuring TiN.

CRediT authorship contribution statement

Clara Saetta: Investigation, Formal analysis, Data curation. **Alessandro Bonardi:** Investigation, Formal analysis, Data curation. **Riccardo Todisco:** Writing – review & editing, Investigation. **Ilaria Barlocco:** Writing – review & editing, Investigation, Formal analysis, Data curation. **Alberto Villa:** Writing – review & editing, Supervision. **Alessandro Morittu:** Formal analysis, Data curation. **Giovanni Maria Piccini:** Writing – review & editing, Supervision. **Giovanni Di Liberto:** Writing – review & editing, Writing – original draft, Supervision, Project administration, Funding acquisition.

Declaration of competing interest

The authors declare that they have no known competing financial interests or personal relationships that could have appeared to influence the work reported in this paper.

Acknowledgements

We gratefully thank Prof. Gianfranco Pacchioni for useful discussion and for reviewing a draft of this work. We also thank Prof. Michele Parrinello research group, Dr. Umberto Raucci, Dr. Simone Perego, and Dr. Luigi Bonati for useful discussion and suggestions of the preparation and training of the machine learning potential of TiN. GDL has received funding through the PRIN project "SACtoH2" (project code P2022AZETB by the Italian Ministry for Universities and Research (MUR), in the context of the National Recovery and Resilience Plan and co-financed by the European Commission – Next Generation EU (Mission 4, Component 1). Access to the CINECA supercomputing resources was granted via ISCRAB and HPC-Regular access call [94,95].

Appendix A. Supplementary data

Supplementary data to this article can be found online at https://doi.org/10.1016/j.apsusc.2026.167089.

Data availability

The data reported in this article can be found in the cited literature and can be asked to the authors upon reasonable request.

References

[1] H.S. Taylor, Chemical reactions at surfaces, Chem. Rev. 9 (1931) 1–46, https://doi.org/10.1021/cr60032a001.
[2] J.Y. Park, L.R. Baker, G.A. Somorjai, Role of hot electrons and metal–oxide interfaces in surface chemistry and catalytic reactions, Chem. Rev. 115 (2015) 2781–2817, https://doi.org/10.1021/cr400311p.
[3] D.A. Panayotov, J.R. Morris, Surface chemistry of Au/TiO2: thermally and photolytically activated reactions, Surf. Sci. Rep. 71 (2016) 77–271, https://doi.org/10.1016/j.surfrep.2016.01.002.
[4] O.S. Pokrovsky, J. Schott, Surface chemistry and dissolution kinetics of divalent metal carbonates, Environ. Sci. Technol. 36 (2002) 426–432, https://doi.org/10.1021/es010925u.
[5] E.L. Sjöberg, D.T. Rickard, Calcite dissolution kinetics: surface speciation and the origin of the variable pH dependence, Chem. Geol. 42 (1984) 119–136, https://doi.org/10.1016/0009-2541(84)90009-3.
[6] E. Tombácz, pH-dependent surface charging of metal oxides, Period. Polytech. Chem. Eng. 53 (2009) 77, https://doi.org/10.3311/pp.ch.2009-2.08.
[7] C. Sinn, D. Meissner, R. Memming, Charge transfer processes at WSe2 electrodes with pH-controlled stability, J. Electrochem. Soc. 137 (1990) 168–172, https://doi.org/10.1149/1.2086353.
[8] T.W. Hamann, F. Gstrein, B.S. Brunschwig, N.S. Lewis, Measurement of the driving force dependence of interfacial charge-transfer rate constants in response to pH changes at n-ZnO/H2O interfaces, Chem. Phys. 326 (2006) 15–23, https://doi.org/10.1016/j.chemphys.2006.02.027.
[9] W. Ji, Y. Kitahama, X. Han, X. Xue, Y. Ozaki, B. Zhao, pH-dependent SERS by semiconductor-controlled charge-transfer contribution, J. Phys. Chem. C 116 (2012) 24829–24836, https://doi.org/10.1021/jp308805n.
[10] M. Kosmulski, The pH dependent surface charging and points of zero charge. X. Update, Adv. Colloid Interface Sci. 319 (2023) 102973, https://doi.org/10.1016/j.cis.2023.102973.
[11] G. Sposito, On points of zero charge, Environ. Sci. Technol. 33 (1999) 208, https://doi.org/10.1021/es982015r.
[12] P. Li, J. Huang, Y. Hu, S. Chen, Establishment of the potential of zero charge of metals in aqueous solutions: different faces of water revealed by ab initio molecular dynamics simulations, J. Phys. Chem. C 125 (2021) 3972–3979, https://doi.org/10.1021/acs.jpcc.0c11089.
[13] K. Leung, First principles determination of the potential-of-zero-charge in an alumina-coated aluminum/water interface model for corrosion applications, J. Electrochem. Soc. 169 (2022) 081502, https://doi.org/10.1149/1945-7111/ac8506.
[14] T. Mahmood, M.T. Saddique, A. Naeem, P. Westerhoff, S. Mustafa, A. Alum, Comparison of different methods for the point of zero charge determination of NiO, Ind. Eng. Chem. Res. 50 (2011) 10017–10023, https://doi.org/10.1021/ie200271d.
[15] D.A. Sverjensky, Zero-point-of-charge prediction from crystal chemistry and solvation theory, Geochim. Cosmochim. Acta 58 (1994) 3123–3129, https://doi.org/10.1016/0016-7037(94)90184-8.
[16] T. Hiemstra, P. Venema, W.H.V. Riemsdijk, Intrinsic proton affinity of reactive surface groups of metal (hydr)oxides: the bond valence principle, J. Colloid Interface Sci. 184 (1996) 680–692, https://doi.org/10.1006/jcis.1996.0666.
[17] B.R. Bickmore, K.M. Rosso, I.D. Brown, S. Kerisit, Bond-valence constraints on liquid water structure, J. Phys. Chem. A 113 (2009) 1847–1857, https://doi.org/10.1021/jp810364t.
[18] F. Ambrosio, J. Wiktor, A. Pasquarello, PH-dependent surface chemistry from first principles: application to the BiVO4(010)-water interface, ACS Appl. Mater. Interfaces 10 (2018) 10011–10021, https://doi.org/10.1021/acsami.7b16545.
[19] Z. Da He, S. Hanselman, Y.X. Chen, M.T.M. Koper, F. Calle-Vallejo, Importance of solvation for the accurate prediction of oxygen reduction activities of Pt-based electrocatalysts, J. Phys. Chem. Lett. 8 (2017) 2243–2246, https://doi.org/10.1021/acs.jpclett.7b01018.
[20] Z. Ding, A. Selloni, Hydration structure of flat and stepped MgO surfaces, J. Chem. Phys. 154 (2021) 114708, https://doi.org/10.1063/5.0044700.
[21] M. Jia, C. Zhang, S.J. Cox, M. Sprik, J. Cheng, Computing surface acidity constants of proton hopping groups from density functional theory-based molecular dynamics: application to the SnO_2 (110)/H_2O interface, J. Chem. Theory Comput. 16 (2020) 6520–6527, https://doi.org/10.1021/acs.jctc.0c00021.
[22] A. Omranpour, J. Elsner, K.N. Lausch, J. Behler, Machine learning potentials for heterogeneous catalysis, ACS Catal. 15 (2025) 1616–1634, https://doi.org/10.1021/ACSCATAL.4C06717.
[23] A. Glielmo, B.E. Husic, A. Rodriguez, C. Clementi, F. Noé, A. Laio, Unsupervised learning methods for molecular simulation data, Chem. Rev. 121 (2021) 9722–9758, https://doi.org/10.1021/ACS.CHEMREV.0C01195.
[24] P. Montero de Hijes, C. Dellago, R. Jinnouchi, B. Schmiedmayer, G. Kresse, Comparing machine learning potentials for water: Kernel-based regression and Behler-Parrinello neural networks, J. Chem. Phys. 160 (2024) 114107, https://doi.org/10.1063/5.0197105/3277916.
[25] A. Tosello Gardini, U. Raucci, M. Parrinello, Machine learning-driven molecular dynamics unveils a bulk phase transformation driving ammonia synthesis on barium hydride, Nat. Commun. 16 (2025) 2475, https://doi.org/10.1038/s41467-025-57688-8.
[26] M. Liu, J. Wang, J. Hu, P. Liu, H. Niu, X. Yan, J. Li, H. Yan, B. Yang, Y. Sun, C. Chen, G. Kresse, L. Zuo, X.Q. Chen, Layer-by-layer phase transformation in Ti3O5 revealed by machine-learning molecular dynamics simulations, Nat. Commun. 15 (2024) 3079, https://doi.org/10.1038/s41467-024-47422-1.
[27] X. Tian, A. Tosello Gardini, U. Raucci, H. Xiao, Y. Zhuo, M. Parrinello, Electrochemical potential-driven water dynamics control CO2 electroreduction at the Ag/H2O interface, Nat. Commun. 16 (2025) 10636, https://doi.org/10.1038/s41467-025-65630-1.
[28] Z. Guo, F. Ambrosio, A. Pasquarello, Evaluation of photocatalysts for water splitting through combined analysis of surface coverage and energy-level alignment, ACS Catal. 10 (2020) 13186–13195, https://doi.org/10.1021/acscatal.0c03006.
[29] P. Gono, F. Ambrosio, A. Pasquarello, Effect of the solvent on the oxygen evolution reaction at the TiO2-water interface, J. Phys. Chem. C 123 (2019) 18467–18474, https://doi.org/10.1021/acs.jpcc.9b05015.

[30] Y. Dong, Y. Wu, M. Liu, J. Li, Electrocatalysis on shape-controlled titanium nitride nanocrystals for the oxygen reduction reaction, ChemSusChem 6 (2013) 2016–2021, https://doi.org/10.1002/cssc.201300331.

[31] S. Yang, J. Kim, Y.J. Tak, A. Soon, H. Lee, Single-atom catalyst of platinum supported on titanium nitride for selective electrochemical reactions, Angew. Chem. 128 (2016) 2098–2102, https://doi.org/10.1002/ange.201509241.

[32] V. Molinari, C. Giordano, M. Antonietti, D. Esposito, Titanium nitride-nickel nanocomposite as heterogeneous catalyst for the hydrogenolysis of aryl ethers, J. Am. Chem. Soc. 136 (2014) 1758–1761, https://doi.org/10.1021/ja4119412.

[33] Y. Zhang, L. Mascaretti, M. Melchionna, O. Henrotte, Š. Kment, P. Fornasiero, A. Naldoni, Thermoplasmonic in situ fabrication of nanohybrid electrocatalysts over gas diffusion electrodes for enhanced H2O2 electrosynthesis, ACS Catal. 13 (2023) 10205–10216, https://doi.org/10.1021/acscatal.3c01837.

[34] J.P. Valleau, L.K. Cohen, Primitive model electrolytes. I. Grand canonical Monte Carlo computations, J. Chem. Phys. 72 (1980) 5935–5941, https://doi.org/10.1063/1.439092.

[35] K. Heijmans, I.C. Tranca, M.-W. Chang, T.J.H. Vlugt;, S.V. Gaastra-Nedea, D.M. J. Smeulders, Reactive grand-canonical Monte Carlo simulations for modeling hydration of $MgCl_2$, ACS Omega 6 (2021) 32475–32484, https://doi.org/10.1021/acsomega.1c03909.

[36] J. Hafner, Ab-initio simulations of materials using VASP: density-functional theory and beyond, J. Comput. Chem. 29 (2008) 2044–2078, https://doi.org/10.1002/jcc.21057.

[37] J.P. Perdew, K. Burke, M. Ernzerhof, Generalized gradient approximation made simple, Phys. Rev. Lett. 77 (1996) 3865.

[38] G. Kresse, D. Joubert, From ultrasoft pseudopotentials to the projector augmented-wave method, Phys. Rev. B 59 (1999) 1758, https://doi.org/10.1103/PhysRevB.59.1758.

[39] S. Grimme, J. Antony, S. Ehrlich, H. Krieg, A consistent and accurate ab initio parametrization of density functional dispersion correction (DFT-D) for the 94 elements H-Pu, J. Chem. Phys. 132 (2010) 154104, https://doi.org/10.1063/1.3382344.

[40] Z. Lian, F. Dattila, N. López, Stability and lifetime of diffusion-trapped oxygen in oxide-derived copper CO2 reduction electrocatalysts, Nat. Catal. 7 (2024) 401–411, https://doi.org/10.1038/s41929-024-01132-5.

[41] M.C.O. Monteiro, F. Dattila, B. Hagedoorn, R. García-Muelas, N. López, M.T. M. Koper, Absence of CO2 electroreduction on copper, gold and silver electrodes without metal cations in solution, Nat. Catal. 4 (2021) 654–662, https://doi.org/10.1038/s41929-021-00655-5.

[42] W.G. Hoover, Canonical dynamics: equilibrium phase-space distributions, Phys. Rev. A (Coll. Park). 31 (1985) 1695–1697, https://doi.org/10.1103/PhysRevA.31.1695.

[43] S. Nosé, A unified formulation of the constant temperature molecular dynamics methods, J. Chem. Phys. 81 (1984) 511–519, https://doi.org/10.1063/1.447334.

[44] L.-M. Liu, C. Zhang, G. Thornton, A. Michaelides, Reply to "comment on 'Structure and dynamics of liquid water on rutile TiO_2 (110)' ", Phys. Rev. B 85 (2012) 167402 https://doi.org/10.1103/PhysRevB.85.167402.

[45] L.-M. Liu, C. Zhang, G. Thornton, A. Michaelides, Structure and dynamics of liquid water on rutile TiO_2 (110), Phys. Rev. B 82 (2010) 161415, https://doi.org/10.1103/PhysRevB.82.161415.

[46] G. Di Liberto, G. Pacchioni, Y. Shao-Horn, L. Giordano, Role of water solvation on the key intermediates catalyzing oxygen evolution on RuO2, J. Phys. Chem. C 127 (2023) 10127–10133, https://doi.org/10.1021/acs.jpcc.3c02733.

[47] F. Maleki, G. Di Liberto, G. Pacchioni, pH- and facet-dependent surface chemistry of TiO2 in aqueous environment from first principles, ACS Appl. Mater. Interfaces 15 (2023) 11216–11224, https://doi.org/10.1021/acsami.2c19273.

[48] N. Daelman, M. Capdevila-Cortada, N. López, Dynamic charge and oxidation state of Pt/CeO2 single-atom catalysts, Nat. Mater. 18 (2019) 1215–1221, https://doi.org/10.1038/s41563-019-0444-y.

[49] M.C.O. Monteiro, F. Dattila, N. López, M.T.M. Koper, The role of cation acidity on the competition between hydrogen evolution and CO2 reduction on gold electrodes, J. Am. Chem. Soc. 144 (2022) 1589–1602, https://doi.org/10.1021/jacs.1c10171.

[50] R.Q. Zhang, T.H. Lee, B.D. Yu, C. Stampfl, A. Soon, The role of titanium nitride supports for single-atom platinum-based catalysts in fuel cell technology, Phys. Chem. Chem. Phys. 14 (2012) 16552–16557, https://doi.org/10.1039/c2cp41392b.

[51] M. Marlo, V. Milman, Density-functional study of bulk and surface properties of titanium nitride using different exchange-correlation functionals, Phys. Rev. B 62 (2000) 2899–2907, https://doi.org/10.1103/PhysRevB.62.2899.

[52] C. Saetta, I. Barlocco, G. Di Liberto, G. Pacchioni, Key ingredients for the screening of single atom catalysts for the hydrogen evolution reaction: the case of titanium nitride, Small 20 (2024) 2401058, https://doi.org/10.1002/smll.202401058.

[53] T. Lee, B. Delley, C. Stampfl, A. Soon, Environment-dependent nanomorphology of TiN: the influence of surface vacancies, Nanoscale 4 (2012) 5183, https://doi.org/10.1039/c2nr31266b.

[54] R.S. Koster, C.M. Fang, M. Dijkstra, A. van Blaaderen, M.A. van Huis, Stabilization of rock salt ZnO nanocrystals by low-energy surfaces and Mg additions: a first-principles study, J. Phys. Chem. C 119 (2015) 5648–5656, https://doi.org/10.1021/jp511503b.

[55] P. Geysermans, F. Finocchi, J. Goniakowski, R. Hacquart, J. Jupille, Combination of (100), (110) and (111) facets in MgO crystals shapes from dry to wet environment, Phys. Chem. Chem. Phys. 11 (2009) 2228, https://doi.org/10.1039/b812376d.

[56] V.K. Lazarov, R. Plass, H.-C. Poon, D.K. Saldin, M. Weinert, S.A. Chambers, M. Gajdardziska-Josifovska, Structure of the hydrogen-stabilized MgO (111) – (1 X 1) polar surface: integrated experimental and theoretical studies, Phys. Rev. B 71 (2005) 115434, https://doi.org/10.1103/PhysRevB.71.115434.

[57] V.K. Lazarov, Z. Cai, K. Yoshida, K.H.L. Zhang, M. Weinert, K.S. Ziemer, P. J. Hasnip, Dynamically stabilized growth of polar oxides: the case of MgO(111), Phys. Rev. Lett. 107 (2011) 056101, https://doi.org/10.1103/PhysRevLett.107.056101.

[58] A.P. Thompson, H.M. Aktulga, R. Berger, D.S. Bolintineanu, W.M. Brown, P. S. Crozier, P.J. in 't Veld, A. Kohlmeyer, S.G. Moore, T.D. Nguyen, R. Shan, M. J. Stevens, J. Tranchida, C. Trott, S.J. Plimpton, LAMMPS – a flexible simulation tool for particle-based materials modeling at the atomic, meso, and continuum scales, Comput. Phys. Commun. 271 (2022) 108171, https://doi.org/10.1016/J.CPC.2021.108171.

[59] I. Batatia, D.P. Kovács, G.N.C. Simm, C. Ortner, G. Csányi, MACE: higher order equivariant message passing neural networks for fast and accurate force fields, Adv. Neural Inf. Process. Syst. 35 (2022) 11423–11436.

[60] I. Batatia, P. Benner, Y. Chiang, A.M. Elena, D.P. Kovács, J. Riebesell, X. R. Advincula, M. Asta, M. Avaylon, W.J. Baldwin, F. Berger, N. Bernstein, A. Bhowmik, F. Bigi, S.M. Blau, V. Cărare, M. Ceriotti, S. Chong, J.P. Darby, S. De, F. Della Pia, V.L. Deringer, R. Elijošius, Z. El-Machachi, E. Fako, F. Falcioni, A. C. Ferrari, J.L.A. Gardner, M.J. Gawkowski, A. Genreith-Schriever, J. George, R.E. A. Goodall, J. Grandel, C.P. Grey, P. Grigorev, S. Han, W. Handley, H.H. Heenen, K. Hermansson, C.H. Ho, S. Hofmann, C. Holm, J. Jaafar, K.S. Jakob, H. Jung, V. Kapil, A.D. Kaplan, N. Karimitari, J.R. Kermode, P. Kourtis, N. Kroupa, J. Kullgren, M.C. Kuner, D. Kuryla, G. Liepuoniute, C. Lin, J.T. Margraf, I. B. Magdău, A. Michaelides, J.H. Moore, A.A. Naik, S.P. Niblett, S.W. Norwood, N. O'Neill, C. Ortner, K.A. Persson, K. Reuter, A.S. Rosen, L.A.M. Rosset, L. L. Schaaf, C. Schran, B.X. Shi, E. Sivonxay, T.K. Stenczel, C. Sutton, V. Svahn, T. D. Swinburne, J. Tilly, C. van der Oord, S. Vargas, E. Varga-Umbrich, T. Vegge, M. Vondrák, Y. Wang, W.C. Witt, T. Wolf, F. Zills, G. Csányi, A foundation model for atomistic materials chemistry, J. Chem. Phys. 163 (2025) 184110, https://doi.org/10.1063/5.0297006/3372267.

[61] H. Kaur, F. Della Pia, I. Batatia, X.R. Advincula, B.X. Shi, J. Lan, G. Csányi, A. Michaelides, V. Kapil, Data-efficient fine-tuning of foundational models for first-principles quality sublimation enthalpies, Faraday Discuss. 256 (2025) 120–138, https://doi.org/10.1039/D4FD00107A.

[62] H. Hussain, G. Tocci, T. Woolcot, X. Torrelles, C.L. Pang, D.S. Humphrey, C.M. Yim, D.C. Grinter, G. Cabailh, O. Bikondoa, R. Lindsay, J. Zegenhagen, A. Michaelides, G. Thornton, Structure of a model TiO2 photocatalytic interface, Nat. Mater. 16 (2017) 461–466, https://doi.org/10.1038/nmat4793.

[63] J.K. Nørskov, T. Bligaard, J. Rossmeisl, C.H. Christensen, Towards the computational design of solid catalysts, Nat. Chem. 1 (2009) 37–46, https://doi.org/10.1038/nchem.121.

[64] M.T. Tang, X. Liu, Y. Ji, J.K. Norskov, K. Chan, Modeling hydrogen evolution reaction kinetics through explicit water–metal interfaces, J. Phys. Chem. C 124 (2020) 28083.

[65] J. Greeley, J.K. Nørskov, Large-scale, density functional theory-based screening of alloys for hydrogen evolution, Surf. Sci. 601 (2007) 1590.

[66] E. Skúlason, V. Tripkovic, M.E. Björketun, S. Gudmundsdóttir, G. Karlberg, J. Rossmeisl, T. Bligaard, H. Jónsson, J.K. Nørskov, Modeling the electrochemical hydrogen oxidation and evolution reactions on the basis of density functional theory calculations, J. Phys. Chem. C 114 (2010) 18182–18197, https://doi.org/10.1021/jp1048887.

[67] J.K. Nørskov, T. Bligaard, A. Logadottir, J.R. Kitchin, J.G. Chen, S. Pandelov, U. Stimming, Trends in the exchange current for hydrogen evolution, J. Electrochem. Soc. 152 (2005) J23.

[68] J.K. Nørskov, J. Rossmeisl, A. Logadottir, L. Lindqvist, J.R. Kitchin, T. Bligaard, H. Jónsson, Origin of the overpotential for oxygen reduction at a fuel-cell cathode, J. Phys. Chem. B 108 (2004) 17886–17892, https://doi.org/10.1021/jp047349j.

[69] C. Mongay, V. Cerdà, A Britton-Robinson buffer of known ionic strength, Ann. Chim. 64 (1974) 409–412.

[70] R.W.G. Wyckoff, Crystal Structures: 1, second ed., Interscience Publishers, New York, 1963, pp. 85–237.

[71] D. Caprion, H.R. Schober, Structure and relaxation in liquid and amorphous selenium, Phys. Rev. B 62 (2000) 3709–3716, https://doi.org/10.1103/PhysRevB.62.3709.

[72] G. Di Liberto, F. Maleki, G. Pacchioni, pH dependence of MgO, TiO_2, and γ-Al_2O_3 surface chemistry from first principles, J. Phys. Chem. C 126 (2022) 10216–10223, https://doi.org/10.1021/acs.jpcc.2c02289.

[73] Z. Ding, Z.K. Goldsmith, A. Selloni, Pathways for electron transfer at MgO–water interfaces from ab initio molecular dynamics, J. Am. Chem. Soc. 144 (2022) 2002–2009, https://doi.org/10.1021/JACS.1C13250.

[74] A.P. Bartók, R. Kondor, G. Csányi, On representing chemical environments, Phys. Rev. B 87 (2013) 184115, https://doi.org/10.1103/PhysRevB.87.184115.

[75] Z. Guo, F. Ambrosio, W. Chen, P. Gono, A. Pasquarello, Alignment of redox levels at semiconductor–water interfaces, Chem. Mater. 30 (2017) 94–111, https://doi.org/10.1021/ACS.CHEMMATER.7B02619.

[76] F. Ambrosio, J. Wiktor, A. Pasquarello, pH-dependent catalytic reaction pathway for water splitting at the BiVO4–water interface from the band alignment, ACS Energy Lett. 3 (2018) 829–834, https://doi.org/10.1021/ACSENERGYLETT.8B00104.

[77] S. Kamble, S. Agrawal, S. Cherumukkil, V. Sharma, R.V. Jasra, P. Munshi, Revisiting zeta potential, the key feature of interfacial phenomena, with applications and recent advancements, ChemistrySelect 7 (2022) e202103084, https://doi.org/10.1002/slct.202103084.

[78] J. Rodriguez-Loya, M. Lerma, J.L. Gardea-Torresdey, Dynamic light scattering and its application to control nanoparticle aggregation in colloidal systems: a review, Micromachines (Basel) 15 (2024), https://doi.org/10.3390/mi15010024.
[79] S. Shrestha, B. Wang, P. Dutta, Nanoparticle processing: understanding and controlling aggregation, Adv. Colloid Interface Sci. 279 (2020) 102162, https://doi.org/10.1016/j.cis.2020.102162.
[80] C.-J. Shih, B.-H. Lung, M.-H. Hon, Colloidal processing of titanium nitride with poly-(methacrylic acid) polyelectrolyte, Mater. Chem. Phys. 60 (1999) 150–157, https://doi.org/10.1016/S0254-0584(99)00063-2.
[81] X. Bai, X. Shi, L. Xu, F. Huang, C. Zheng, L. Xu, B. Li, Q. Wang, Effects of hydrothermal treatment on physicochemical and anticorrosion properties of titanium nitride coating on pure titanium, Appl. Surf. Sci. 507 (2020) 145030, https://doi.org/10.1016/J.APSUSC.2019.145030.
[82] I.G. Polyakova, T. Hübert, Thermal stability of TiN thin films investigated by DTG/DTA, Surf. Coat. Technol. 141 (2001) 55–61, https://doi.org/10.1016/S0257-8972(01)01042-8.
[83] M. Wittmer, J. Noser, H. Melchior, Oxidation kinetics of TiN thin films, J. Appl. Phys. 52 (1981) 6659–6664, https://doi.org/10.1063/1.328659.
[84] G. Di Liberto, Á. Morales-García, S.T. Bromley, An unconstrained approach to systematic structural and energetic screening of materials interfaces, Nat. Commun. 13 (2022) 6236, https://doi.org/10.1038/s41467-022-33414-6.
[85] G. Di Liberto, L.A. Cipriano, S. Tosoni, G. Pacchioni, Rational design of semiconductor heterojunctions for photocatalysis, Chem. A Eur. J. 27 (2021) 13306–13317, https://doi.org/10.1002/CHEM.202101764.
[86] L.A. Cipriano, G. Di Liberto, S. Tosoni, G. Pacchioni, Structure and band alignment of InP photocatalysts passivated by TiO2 thin films, J. Phys. Chem. C 125 (2021) 11620–11627, https://doi.org/10.1021/ACS.JPCC.1C01666.
[87] Y.Q. Zhou, Z. Guo, J. Bi, J.T. Ye, M. Ge, Y. Lin, S. Xiao, Y. Cao, L. Wang, L.F. Huang, Unifying the atomistic trends for early-stage evolution of TiN surfaces in atmospheric and aqueous environments, Acta Mater. 289 (2025) 120909, https://doi.org/10.1016/J.ACTAMAT.2025.120909.